Role of quadratic and cubic spectral phases in ladder climbing with ultrashort pulses

Béatrice Chatel, Jérôme Degert, Bertrand Girard

Role of quadratic and cubic spectral phases in ladder climbing with ultrashort pulses

Béatrice Chatel, Jérôme Degert, and Bertrand Girard
Laboratoire de Collisions, Agrégats, Réactivité (CNRS UMR 5589), IRSAMC Université Paul Sabatier, 31062 Toulouse, France
(Received 13 July 2004; published 30 November 2004)

Two-photon excitation of a quantum ladder system by an ultrashort chirped pulse leads to interferences in the excited-state population, between direct and sequential paths. Experimental results have been obtained in atomic sodium vapor. The presence of several intermediate and final states leads to new phenomena. The interplay between the two sequential paths leads to strongly contrasted oscillations and a large enhancement of the transition probability for precise values of the chirp. A cubic spectral phase modifies significantly the behavior of the quantum interferences and can be used to enhance the two-photon absorption rate.

DOI: 10.1103/PhysRevA.70.053414 PACS number(s): 32.80.Wr, 32.80.Qk, 42.65.Re, 78.47.+p

I. INTRODUCTION

Coherent control of atomic and molecular processes has been a widely expanding field in the past two decades. One initial goal was set by chemical physicists to achieve selectivity and enhancement of chemical reactions [1–7]. Many different schemes have so far been proposed and demonstrated experimentally, and most of them rely on the intrinsic coherence properties of lasers. The quantum interferences between excitation induced by a laser field and by its second or third harmonics were among the first schemes to achieve spectacular results: control of an absolute excitation cross section [8,9], of the branching ratio between two chemical processes [10], or of the direction of photocurrents [11,12]. Another approach based on stimulated adiabatic passage (STIRAP) has also been widely developed [13,14].

With ultrashort pulses, the pump-probe [15,16], pump-dump-probe [17] or pump-control-probe [18] are the simplest approaches which require only "internal" coherence of the different spectral components contained in each Fourier-transform-limited pulse. Schemes based on a pair or a sequence of identical pulses rely on interferences between the quantum paths associated with each pulse and which connect the same initial state with the same final state [19–29]. This is analogous to Ramsey fringes well studied and used in high-resolution spectroscopy. Another family of control strategy relies on a "single" coherent pulse whose spectral phase and/or amplitude is modified with dispersive devices or shaped [30]. This last approach is often called the optimal control strategy when it is associated with an optimization algorithm within a closed loop [31–34]. It was strongly developed after the technological breakthrough for generating arbitrarily shaped pulses [35,36]. It can also be used in an open-loop strategy where the desired pulse shape is chosen after a theoretical analysis of the interaction [37–44]. This open-loop approach is well adapted to small systems for which theoretical predictions are reliable.

Quantum ladder climbing is a particular situation which finds a straightforward application in the vibrational excitation of molecules [45–52] or in their rotational excitation through a succession of Raman transitions [53,54]. Ladder climbing combines multiphoton transitions and sequential one-photon transitions. It can be performed in the weak-field as well as in the strong-field regime, with Fourier-limited pulses, chirped pulses [55–59], or shaped pulses [40]. Alkali atoms have a natural electronic ladder with three nearly equidistant levels. They provide therefore a benchmark system in which new excitation schemes can be explored. This paper presents a detailed study of interference effects in ladder climbing with chirped pulses having quadratic and cubic spectral phase.

In the low-field regime, Meshulach and Silberberg have demonstrated that Fourier-transform-limited pulses are optimal for two-photon transitions without intermediate states [37,38] but not for two-photon transitions with a nearly resonant intermediate state [40]. Furthermore, in such a ladder system one can observe interferences between sequential and direct two-photon transitions. Balling *et al.* have proposed a scheme using a linearly chirped pulse to excite a two-photon transition in rubidium [56]. Recently a new analytic approach of this scheme has been proposed by Chatel *et al.* and applied to Na($3s$-$3p$-$5s$) [59]. In this work two intermediate states were present, providing new interference paths. In particular, the interference between two sequential paths has a chirp-independent contrast and presents analogies with pump-probe experiments. This paper presents a detailed account of these results and extends them to the case where several final states can be reached. Effectively, new interference patterns are present. Varying the excitation wavelength changes their weight but leads also to a qualitatively unexpected behavior. Higher-order terms in the phase development have to be included to explain these observations.

In this paper, we first recall the basic model of a ladder climbing excitation by a linearly chirped pulse (Sec. II). In Sec. III, we detail the role of several intermediate and final states in the quantum interference pattern. The sodium atom is chosen to illustrate this scheme. Due to the broad bandwidth of the excitation laser pulse, two different two-photon transitions are excited. The experimental setup and results are presented in Sec. IV. Finally in the last part the role of the cubic phase is investigated and explained using the Wigner representation.

II. BASIC MODEL: ONE INTERMEDIATE AND ONE FINAL STATE

We first recall the origin of the interferences for the simple case of a two-photon transition involving three

atomic levels: the ground state $|g\rangle$, one intermediate state $|k\rangle$, and the excited state $|e\rangle$. $\omega_{kg}=(E_k-E_g)/\hbar$ and $\omega_{ek}=(E_e-E_k)/\hbar$ are the corresponding one-photon transition frequencies. $\omega_{eg}=(E_e-E_g)/\hbar$ is the two-photon transition frequency. This ladder system is excited by a weak ultrashort pulse $\mathcal{E}(t)$, of Fourier transform $E(\omega)$. The carrier frequency is ω_0 and is tuned on the two-photon resonance $2\omega_0=\omega_{eg}$. The one-photon detuning $\delta=\omega_{kg}-\omega_0$ is smaller than or comparable to the spectral bandwidth, but nonzero ($0<|\delta|\lesssim\delta\omega_L$) so that these three levels constitute an approximate ladder. The overall pulse duration is assumed here to be considerably shorter (picosecond scale) than all lifetimes (nanosecond scale) involved. Therefore, damping can be neglected and the Schrödinger equation can be used. The general expression of the excited-state amplitude, for a two-photon transition involving a nearly resonant intermediate level, can be written as [40]

$$a_e=-\frac{\mu_{ek}\mu_{kg}}{\hbar^2}\left[\frac{1}{2}E(\omega_{kg})E(\omega_{ek})+\frac{i}{2\pi}\mathrm{P}\int_{-\infty}^{+\infty}d\omega\frac{E(\omega)E(\omega_{eg}-\omega)}{\omega-\omega_{kg}}\right], \tag{1}$$

where μ_{ij} is the dipole moment matrix element between states $|i\rangle$ and $|j\rangle$, P is the principal Cauchy value.

In this section, we focus our study on the particular case of linearly chirped Gaussian pulses. The spectral phase is

$$\phi(\omega)=\phi_0+\phi''(\omega-\omega_0)^2/2, \tag{2}$$

where ϕ'' is the quadratic phase or second-order dispersion. Since only one pulse is present, with a duration much longer than the optical cycle, ϕ_0 can be set to zero without loss of generality. This would not be the case for ultrashort pulses of a few optical cycles for which carrier envelope phase effects have been seen to have major effects in strong-field experiments [60–62]. The electric field is thus given by

$$E(\omega)=\sqrt{\pi}\mathcal{E}_0T_0e^{-(\omega-\omega_0)^2T_0^2/4}e^{i\phi''(\omega-\omega_0)^2/2}, \tag{3}$$

where $2T_0$ is the field-transform-limited temporal width (at $1/e$), $\delta\omega_L=4/T_0$ the field spectral width, and ϕ'' the quadratic phase dispersion inducing the linear chirp. The corresponding temporal electric field is given (in the rotating-wave approximation) by

$$\mathcal{E}(t)=\frac{1}{2}\mathcal{E}_0\sqrt{\frac{\Gamma}{\Gamma_0}}e^{-\Gamma t^2}e^{-i\omega_0t}, \tag{4}$$

with $1/\Gamma=1/\Gamma_0-2i\phi''$ and $1/\Gamma_0=T_0^2$. The chirped pulse width is therefore given by

$$T_p=T_0\sqrt{1+(2\phi''/T_0^2)^2}. \tag{5}$$

The instantaneous frequency varies linearly with time during the pulse:

$$\omega(t)=\omega_0+2\alpha t, \tag{6}$$

where

$$\alpha=\frac{2\phi''}{{T_0}^4+(2\phi'')^2}. \tag{7}$$

Expression (1) can be written using the complex error function:

$$a_e=-\frac{\mu_{ek}\mu_{kg}}{2\hbar^2}E(\omega_{kg})E(\omega_{ek})\left[1-\mathrm{erf}\left(i\frac{\delta}{\sqrt{2\Gamma}}\right)\right]. \tag{8}$$

The error function oscillates as a function of its argument. However, this exact expression does not provide any direct physical insight. In our previous work [59], it has been shown that for large chirps ($|\phi''|\gg T_0^2$), Eq. (1) can be separated into two distinct contributions: one is due to the direct two-photon transition while the second one is due to the sequential process. Two frequency ranges provide major contributions to the second term in Eq. (1), around ω_0 and ω_{kg}, respectively. The first one results from the stationary-phase approximation and gives the direct two-photon transition amplitude a_d. It corresponds to a small range of frequencies ($\Delta\omega\simeq 1/\sqrt{|\phi''|}$) centered on ω_0 that can fulfill the two-photon resonance condition. The second one is due to the pole in the principal Cauchy value and provides a second significant contribution, identical to the sequential contribution already present in Eq. (1), except for its sign which depends on the sign of ϕ''. Finally one obtains the probability amplitude $a_e\simeq a_s+a_d$, with

$$a_s=-\frac{\mu_{ek}\mu_{kg}}{\hbar^2}E(\omega_{ek})E(\omega_{kg})\frac{1-\mathrm{sgn}(\phi''\delta)}{2}, \tag{9a}$$

$$a_d=-\frac{\mu_{ek}\mu_{kg}}{\hbar^2}\frac{E^2(\omega_0)}{\delta\sqrt{2\pi T_0T_p}}e^{-i(\theta+\pi)/2}, \tag{9b}$$

where a_s and a_d are the sequential and direct contributions, respectively, and $\tan\theta=-2\phi''/T_0^2$. Note that a_d corresponds exactly to the nonresonant excited-state amplitude [38,40] with a far-off-resonance intermediate state. $|a_d|^2$ is plotted in Fig. 1 (dashed line). It decreases as $\simeq 1/T_p$ or $1/\sqrt{1+(2\phi''/T_0^2)^2}$ [see Eq. (5)] and has a full width at half maximum (FWHM) of $T_0^2\sqrt{3}$. The sequential contribution probability $|a_s|^2$ [Eq. (9a)] is a steplike function (dash-dotted line in Fig. 1) depending only on the power spectrum at each one-photon transition. The sharp increase around zero chirp occurs when the frequencies of the pulse arrive in the intuitive order (ω_{kg} before ω_{ek}): excitation of the intermediate state $|k\rangle$ *followed* by excitation from $|k\rangle$ to $|e\rangle$.

A chirp-dependent phase factor $e^{i\phi''\delta^2}$, arising from the electric field [see Eq. (3)], is present in the sequential term [Eq. (9a)]. The phase factor $e^{-i(\theta+\pi)/2}$ contained in the direct contribution varies only for small chirps, $|\phi''|\lesssim T_0^2$ (from $-3\pi/4$ for $\phi''<-T_0^2$ to $-\pi/4$ for $\phi''>T_0^2$). This phase difference accumulated between both paths leads to strong interferences in the excited-state population $|a_e|^2$ as a function of the quadratic phase dispersion ϕ'' as shown in Fig. 1 (solid line). Depending on the sign of the one-photon detuning δ, the interferences occur either for positive or negative chirp. The period of the corresponding oscillations is thus equal to $\phi''_{2\pi}=2\pi/\delta^2$. In Fig. 1 the analytic approximation of $|a_e|^2$

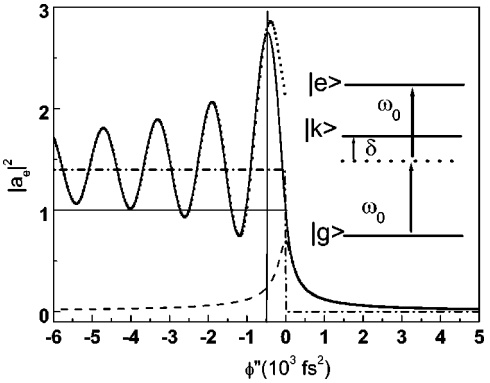

FIG. 1. Population of the excited state as a function of chirp for $\delta>0$, normalized to the population achieved with a FT-limited pulse ($\phi''=0$). Dash-dotted line: sequential contribution $|a_s|^2$. Dashed line: direct contribution $|a_d|^2$. Total two-photon contribution $|a_e|^2$, using the exact expression given by Eq. (8) (solid line) and its approximation, Eq. (9) (dots). Inset: three-level system, where ω_0 is the carrier frequency of the laser and δ the detuning with respect to the intermediate state $|k\rangle$. The vertical line corresponds to $\phi''=-3\pi/4\delta^2$.

[Eq. (9)] is plotted with dots (for $\delta>0$ and $\delta/\delta\omega_L\simeq 0.5$). The agreement with the exact expression (solid line) given by Eq. (8) is excellent, except for the small region around zero chirp ($|\phi''|\lesssim 1/\delta^2$) where the approximation is not valid. For $\phi''>0$, $|a_e|^2$ has the same behavior as $|a_d|^2$. On the other hand, for $\phi''<0$ the population oscillates strongly around $|a_s|^2$. The first maximum is reached when both amplitudes have nearly the same phase factors—i.e., for $\phi''\simeq -3\pi/4\delta^2$ [this value is only approximate since the variation of magnitude of a_d is not taken into account and since this is at the limit of validity of the approximation made to derive Eq. (9)]. These interferences were first observed experimentally by Balling *et al.* in Rb [56] with a reduced contrast.

III. QUANTUM LADDER WITH SEVERAL INTERMEDIATE STATES AND FINAL STATES

We consider in this section the cases of several intermediate and final states. Adding new paths leads to multiple interferences. However, one has to distinguish new intermediate states and new final states. The first case provides new coherent paths sharing the same final state. They interfere therefore together. The contributions towards different final states are incoherent and need to be summed separately. Each case is discussed in the following subsections.

A. Two intermediate states

We consider the case of two intermediate states $|k_1\rangle$, $|k_2\rangle$ contributing to the two-photon transition. The generalization to more than two levels is immediate. One assumes that the detunings $\delta^{(k)}=\omega_{kg}-\omega_{eg}/2$ (for $k=k_1,k_2$) are smaller than or comparable to the spectral bandwidth and have the same signs. The expression of the excited-state amplitude is directly derived from Eq. (8) by summing over the two intermediate levels:

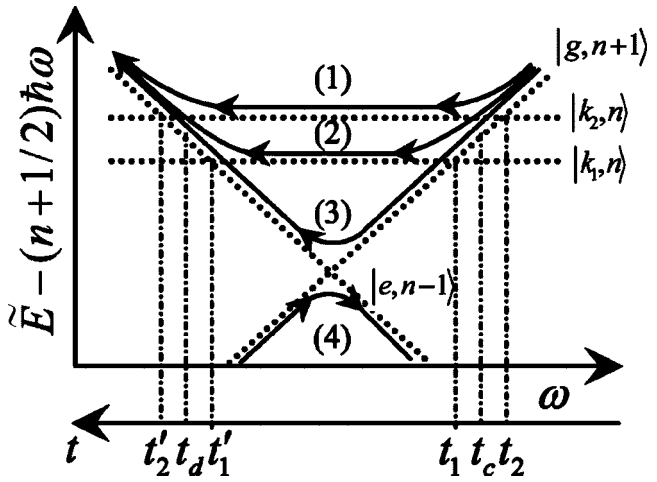

FIG. 2. Dressed-state picture of a ladder system with two intermediate states. The arrows indicate the different paths. For a negative chirp, the frequency decreases with time and paths (1)–(3) are followed as indicated by the arrow of time. The crossing between states $|k_i,n\rangle$ and $|g,n+1\rangle$ ($|e,n-1\rangle$) is reached at time t_i (t_i'). Time t_c is the apparent creation time of the wave packet, whereas t_d is the apparent detection time (see text).

$$a_e=-\frac{1}{2\hbar^2}\sum_{k=k_1,k_2}\mu_{ek}\mu_{kg}E(\omega_{ek})E(\omega_{kg})\times\left[1-\mathrm{erf}\left(i\frac{\delta^{(k)}}{\sqrt{2\Gamma}}\right)\right]. \tag{10}$$

In the case of large chirps ($|\phi''|\gg T_0^2$), we can use the same approximation as in Sec. II. Two sequential paths a_{s_1} and a_{s_2} are now present where

$$a_{s_i}=-\frac{\mu_{ek_i}\mu_{k_ig}}{\hbar^2}E(\omega_{ek_i})E(\omega_{k_ig})\frac{1-\mathrm{sgn}(\phi''\delta^{(k_i)})}{2}. \tag{11}$$

Each sequential path can now interfere with the direct path. Moreover, the two sequential paths can also interfere together.

These interferences can be easily explained by using the dressed state picture (see Fig. 2) which takes correctly into account the coupled evolution of the atom and field, even in the perturbation regime. The dressed atomic states are $|a,n\rangle$ where $|a\rangle$ is an atomic state and $|n\rangle$ the photon number state. Their energy is given by $\tilde{E}_{n,a}=E_a+\left(n+\frac{1}{2}\right)\hbar\omega+E_{int}$ where E_{int} is the interaction energy. A given manifold of neighboring energy consists of $|g,n+1\rangle$, $|k_i,n\rangle(i=1,2)$ and $|e,n-1\rangle$. The dashed lines in Fig. 2 represent the diabatic states, the solid lines the quantum paths (which follow the adiabatic states obtained by including the atom-field coupling).

For a positively (negatively) chirped pulse, the temporal evolution of the system corresponds to a crossing of the diagram from left to right (from right to left). At each crossing, the wave packet splits into two components of relative magnitude depending on the coupling strength. Here in the weak-field regime, the major component remains on the diabatic curve. The two sequential paths (1) and (2) correspond to two successive one-photon transitions leading to the state $|e,n-1\rangle$. They can be followed only for negative chirp. Paths

(3) and (4) are the direct two-photon transitions for negative and positive chirp, respectively. Each path (j) contributes to the final-state probability amplitude as $|a_j|\exp(-i\varphi_j)$ where a_j depends on the Rabi pulsation and the chirp. φ_j is the phase accumulated along the path. As all the path contributions add coherently together, the population in the final state can be written as

$$P_e = P_1 + P_2 + P_3 + 2\sqrt{P_1P_2}\cos\Delta\varphi_{21} + 2\sqrt{P_2P_3}\cos\Delta\varphi_{32} + 2\sqrt{P_1P_3}\cos\Delta\varphi_{31}, \quad (12)$$

where $P_j=|a_j|^2$ and $\Delta\varphi_{ji}=\varphi_j-\varphi_i$. Depending on the value of the relative phase, the interference term $\cos\Delta\varphi_{ij}$ leads to strong oscillations (see Fig. 5). P_e is the sum of these three interference patterns. The period of each pattern can be easily determined in the dressed-state picture. The relative phase $\Delta\varphi_{ij}$ between paths (i) and (j) is given by $\hbar\Delta\varphi_{ij}=\int[\tilde{E}_i(t)-\tilde{E}_j(t)]dt$ which is the product of the chirp rate by the enclosed area delimited by these paths in the dressed-state diagram [55].

When $\Delta\varphi_{ij}$ is a multiple of 2π, then paths (i) and (j) are in phase and result in a maximum contribution to the final population. In the example given below, the one-photon detunings have close values. Therefore the contributions corresponding to the interferences between paths (1) and (3) and between path (2) and (3) lead to oscillations with close short periods inversely proportional to the triangle areas while the contribution of the interferences between both sequential paths (1) and (2) has a slow period inversely proportional to the trapezoid delimited by these paths (Fig. 5).

Note that for small chirps ($|\phi''|\simeq T_0^2$), all the frequencies are simultaneously present. The dressed-level picture with a slow varying frequency is not appropriate to explain the observations. Then the distinction between the sequential and direct two-photon processes is not relevant since all frequencies are "resonant" with the one-photon transitions, within the uncertainty associated to the pulse duration.

After the one-photon transitions associated with the first step, the system is in a superposition of the ground state and the two intermediate states. During the second step, the intermediate states are "excited" towards the final state. This situation is strongly similar to pump-probe experiments. However, an important difference is that here everything happens within one single pulse. The first part of the pulse (the "pump") creates a wave packet in the intermediate states which is probed by the second part of the pulse. The evolution of the wave packet is described by the relative phases between the states of the superposition. These phase differences are usually evaluated with the bare states, but this is only valid for a free evolution of the system between pump and probe and should thus be avoided here. However, since here the pump and probe steps are performed within the same laser pulse whose frequency evolves in time, calculation of the pump-probe signal should take into account this phase variation of the pulse. The dressed-state formalism includes both atomic and field evolution and should therefore be used.

State $|k_i\rangle$ is created at time t_i and probed at time $t_i'(i=1,2)$. The phase difference between the two paths is given by the area of the trapezoid delimited by them (see Fig. 2). This trapezoid has a long basis given by $t_2'-t_2$ and a small basis given by $t_1'-t_1$. Its area is equal to the area of the rectangle of basis $(t_1'+t_2'-t_1-t_2)/2$. Thus, the system is equivalent to a wave packet, coherent superposition of the two intermediate states, created at $t_c=(t_1+t_2)/2=(\delta_1+\delta_2)\phi''/2$ and detected when the laser frequency reaches the second sequential transition at $t_d=(t_1'+t_2')/2=-(\delta_1+\delta_2)\phi''/2$. The accumulated relative phase between the two levels is $(t_d-t_c)\Delta E/\hbar=(t_d-t_c)(\delta_2-\delta_1)=(\delta_2^2-\delta_1^2)\phi''$ as calculated above. This analogy with pump-probe experiments cannot be extended to more than two intermediate states since the effective creation time of the wave packet is not unique and depends on the pair of intermediate states considered.

B. Several final states

In the experiment described below, the excited-state population is indirectly observed through a radiative cascade. Several excited states can thus contribute to the fluorescence. This is particularly the case with ultrashort pulses which have a broad bandwidth. However, unlike the case of several intermediate levels, these various excited states contribute incoherently to the signal. So the signal is just proportional to $\Sigma C_j|a_j|^2$ where a_j are the excited-state $|e_j\rangle$ probability amplitudes (the excited states which lead to emission of a photon on the fluorescence transition) and C_j their detection probability.

For detunings $\delta_e^{(k)}$ and $\delta_{e'}^{(k)}$ of opposite signs, the sequential contributions associated with each final state $|e\rangle$ and $|e'\rangle$ are present for opposite signs of the chirp (see Figs. 4 and 5). On the contrary, for detunings with the same sign, the sequential contributions and thus the various interference patterns are present for the same sign of the chirp (opposite to the sign of $\delta_e^{(k)}$).

IV. EXPERIMENT

A. Sodium as a benchmark system

The sodium atom is chosen here to illustrate experimentally these multiple interferences. Two intermediate states are involved, and due to the broadness of the laser bandwidth, three final states can be reached. The levels are represented in Fig. 3. The two-photon transitions of interest are $3s$-$5s$ and $3s$-$4d$ ($^2D_{3/2}$ and $^2D_{5/2}$). The intermediate states involved in the two-photon transitions are $3p$ ($^2P_{1/2}$ and $^2P_{3/2}$). The three excited states decay in part towards the $4p$ state and the $4p$ -$3s$ fluorescence is detected. The detection probability C_j of state $|e_j\rangle$ is therefore the product of the two quantum yields (fraction of decay rate towards the $4p$ state by the fraction of decay processes from the $4p$ state towards the $3s$ ground state). The wavelengths and dipole moments of the relevant transitions are recalled in Table I.

Figure 4 represents the dressed-state picture and all the allowed quantum paths. The particularity of this system is that due to the sign of the detunings, the $3s$-$5s$ and $3s$-$4d$

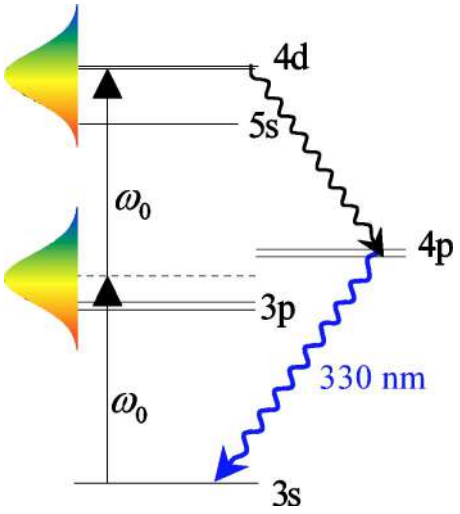

FIG. 3. (Color online) Diagram of the sodium levels involved. The two-photon transition is drawn here on resonance with the 4*d* final state.

two-photon transitions lead to oscillations for negative and positive chirp, respectively, as shown in the numerical simulations presented in Fig. 5. These simulations are performed in the weak-field regime, using Eq. (10) and summing incoherently the contributions towards the various final states. By varying the central wavelength of the laser pulse one can favor one or the other two-photon transition as shown in Fig. 5. At 611 nm [Fig. 5(a)], the 3*s*-5*s* two-photon transition is excited only, whereas the 3*s*-4*d* transition dominates at 574 nm [Fig. 5(d)]. For intermediate wavelengths [Figs. 5(b) and 5(c)], both final states can be reached, with relative weights depending on the spectral intensity at the relevant frequencies.

The 3*s*-4*d* ($^2D_{5/2}$) transition can be excited through the 3*p* ($^2P_{3/2}$) only. Therefore, only one sequential-direct interference (such as described in Sec. II and Fig. 1) is present in the excitation probability towards this final level 4*d* ($^2D_{5/2}$). The other two-photon transitions [3*s*-5*s* and 3*s*-4*d* ($^2D_{3/2}$)] involve both 3*p* ($^2P_{1/2}$ and $^2P_{3/2}$) intermediate states. Therefore, two sequential paths and one direct path are present, leading to three interference contributions. For each final state, the two-photon detuning $\delta_e^{(k_i)}$ is much larger than the

TABLE I. Spectroscopic data concerning the sodium levels involved in the experiment.

Level	Energy (cm^{-1}) [63]	Transition	Wavelength in vacuum (nm)	Dipole moment (C m) [64]
$3s_{1/2}$	0			
$3p_{1/2}$	16956,17	$3s_{1/2}\rightarrow 3p_{1/2}$	589,75	$1,209\times10^{-29}$
$3p_{3/2}$	16973,37	$3s_{1/2}\rightarrow 3p_{3/2}$	589,16	$-1,710\times10^{-29}$
$5s_{1/2}$	33200,68	$3p_{1/2}\rightarrow 5s_{1/2}$	615,59	$-2,558\times10^{-30}$
		$3p_{3/2}\rightarrow 5s_{1/2}$	616,25	$3,620\times10^{-30}$
$4d_{5/2}$	34548,73	$3p_{3/2}\rightarrow 4d_{5/2}$	568,98	$6,892\times10^{-30}$
$4d_{3/2}$	34548,77	$3p_{1/2}\rightarrow 4d_{3/2}$	568,42	$-6,629\times10^{-30}$
		$3p_{3/2}\rightarrow 4d_{3/2}$	568,98	$9,385\times10^{-31}$

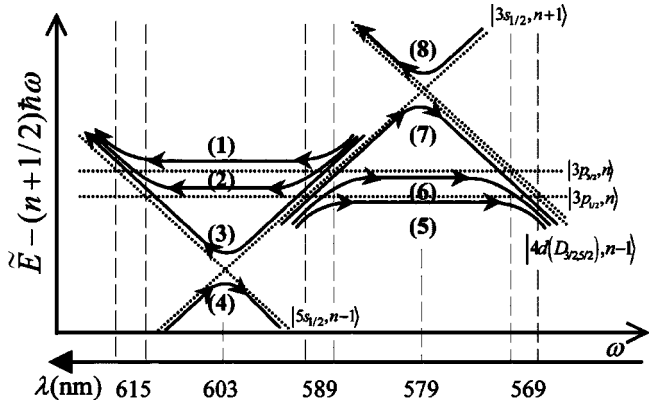

FIG. 4. Sodium levels in the dressed atom picture. Paths 1–4 are associated with the 5*s* final state and paths 5–8 with the 4*d* final state.

intermediate-state splitting: $|\delta_e^{(k_i)}| \gg ||\delta_e^{(k_1)}| - |\delta_e^{(k_2)}||$. Thus two rapid oscillations are due to the interferences between sequential paths (1) and (2) [(5) and (6)] with the direct path (3) [(7)], and one slow oscillation results from interferences between sequential paths (1) and (2) [(5) and (6)]. The values of all the periods of interferences are gathered in Table II. Due to the near degeneracy of the 4*d* doublet, the direct-path—sequential-path interferences [through the common 3*p* ($^2P_{3/2}$) intermediate state] associated with both final states have the same period.

The probability of each path depends on the strength of the coupling at the crossing which is proportional to the laser electric field amplitude and the corresponding dipole moments. The sequential-sequential interference is highly contrasted for balanced excitation paths. Moreover, its amplitude is chirp independent whereas the sequential-direct interference amplitude depends on $\delta/\delta\omega_L$ (see Sec. II) and decreases rapidly with $|\phi''|$. Using expression (12), one can calculate the theoretical contrast of sequential-sequential interference (oscillations with a long period) for negative chirp (3*s*-5*s* transition), assuming the same spectral intensity at each transition:

$$C = \frac{P_{max} - P_{min}}{P_{max} + P_{min}} = \frac{2|a_5||a_6|}{|a_5|^2 + |a_6|^2} = 80\,\%\,, \qquad (13)$$

where

TABLE II. Periods $\phi''_{2\pi}(ji)(fs^2)$ of all the interference paths. Quantum paths are numbered in Fig. 4.

Paths (*ji*)	Interference period $\phi''_{2\pi}(ji)$ (fs^2)
1-3	1273
2-3	1399
1-2	14119
5-7	1749
6-7	1955
5-6	16578

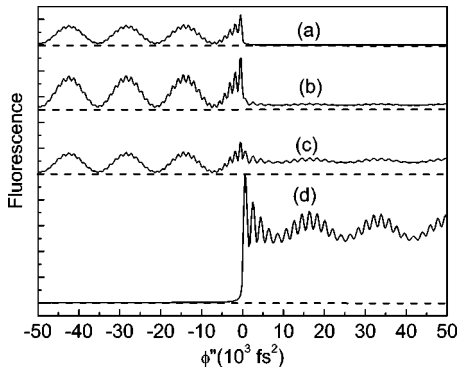

FIG. 5. Calculated $4p$-$3s$ fluorescence as a function of the chirp. The laser parameters have been chosen to be similar to the ones used in the experiment: (a) $\lambda_0=611$ nm ($\delta\lambda=28$ nm), (b) $\lambda_0=599$ nm ($\delta\lambda=24$ nm), (c) $\lambda_0=596$ nm ($\delta\lambda=28$ nm), and (d) $\lambda_0=574$ nm ($\delta\lambda=23$ nm).

$$|a_6| \propto \mu_{3s_{1/2}-3p_{1/2}}\mu_{3p_{1/2}-5s_{1/2}}, \tag{14}$$

$$|a_5| \propto \mu_{3s_{1/2}-3p_{3/2}}\mu_{3p_{3/2}-5s_{1/2}}, \tag{15}$$

as well as for positive chirp ($3s$-$4d$ transition):

$$C = \frac{2|a_1||a_2|}{|a_1|^2+|a_2|^2+|a_2'|^2} = 12\,\%\,, \tag{16}$$

where

$$|a_1| \propto \mu_{3s_{1/2}-3p_{1/2}}\mu_{3p_{1/2}-4d_{3/2}}, \tag{17}$$

$$|a_2| \propto \mu_{3s_{1/2}-3p_{3/2}}\mu_{3p_{3/2}-4d_{3/2}}, \tag{18}$$

$$|a_2'| \propto \mu_{3s_{1/2}-3p_{3/2}}\mu_{3p_{3/2}-4d_{5/2}}. \tag{19}$$

This difference is mainly due to the $4d$ ($^2D_{5/2}$) state which is accessible only through the $3p$ ($^2P_{3/2}$) intermediate state and therefore does not contribute to the sequential-sequential interference, but reduces its contrast.

An analogy with pump-probe experiments was made at the end of Sec. III A. The wave packet created here is a superposition of two $3p$ fine structure states ($^2P_{1/2}$ and $^2P_{3/2}$). It corresponds thus to a spin-orbit precession [25,65–68]. The initial "bright" state is $|L=1, M_L=0\rangle$ with a linear polarization. The dark states are $|L=1, M_L=\pm 1\rangle$ depending on the initial spin sublevel $M_s=\pm 1/2$. For a $5s$ final state and linear polarization, they cannot be excited towards the final state. This explains the much higher contrast observed here for the $3s$-$5s$ transition as compared to $3s$-$4d$ or previous spin precession studies [66–68].

B. Experimental setup

To perform the experiment [59], a conventional Ti: sapphire laser with chirped pulse amplification (Spitfire Spectra Physics) is used. It supplies 800 μJ at a central wavelength of 795 nm with a pulse duration FWHM of 130 fs. The repetition rate is 1 kHz. A fraction of the energy feeds a home-made noncollinear optical parametric amplifier [69], without compression, which delivers pulses of 10 μJ, ca 30 nm bandwidth tunable from 500 nm to 700 nm. To vary the chirp ϕ'' on the interval [$-40\,000$ fs^2, $40\,000$ fs^2] with 100 fs^2 steps, we have combined glass rods (4 cm SF58, 6 cm SF10) with an adjustable double pass gratings pair (600 grooves/mm).

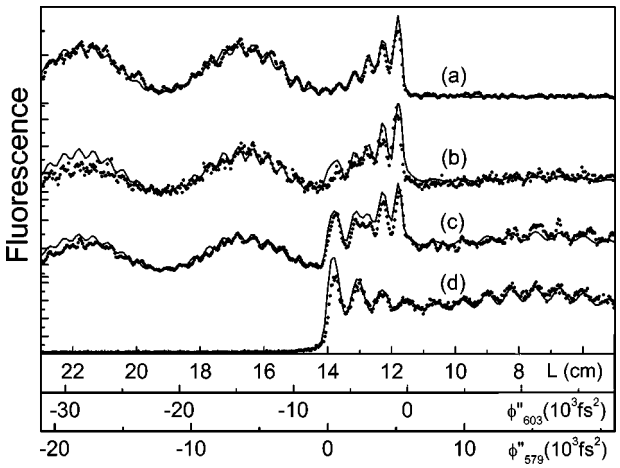

FIG. 6. $4p$-$3s$ fluorescence as a function of the grating's distance L. The values of the chirp ϕ''_λ are also indicated at $\lambda=603$ nm and $\lambda=579$ nm corresponding to the two-photon transitions. Experimental results (dots) with simulations (solid lines). The scans correspond to different wavelengths: (a) $\lambda_0=611$ nm ($\delta\lambda=28$ nm), (b) $\lambda_0=599$ nm ($\delta\lambda=24$ nm), (c) $\lambda_0=596$ nm ($\delta\lambda=28$ nm), and (d) $\lambda_0=574$ nm ($\delta\lambda=23$ nm).

The pulse is slightly focused into a sealed cell containing natural sodium with a pressure of 1.7×10^{-4} Pa. The $4p \rightarrow 3s$ fluorescence signal at 330 nm is collected by 18 optical fibers and detected by a photomultiplier with photon counting. The signal was monitored as a function of the grating's distance, which is essentially proportional to the chirp but not exactly as explained below.

C. Results

The $4p \rightarrow 3s$ fluorescence is plotted in Fig. 6 as a function of the grating's distance for the same excitation wavelengths as in the simulations presented in Fig. 5. The curves at 611 nm and 574 nm involve preferentially a single final state (611 nm corresponds to the $3s$-$5s$ transition while 574 nm corresponds to the $3s$-$4d$ transition). In both cases strong interferences with the small and large periods are observed as described above. The experimental periods as well as the contrast of the oscillations are in perfect agreement with the calculated one. The experimental results in these two cases reproduce perfectly the simulation obtained and plotted in Fig. 5. However, one striking difference shows up when comparing the results obtained at these two wavelengths: The onset of oscillations do not take place at the same grating's distance. At intermediate wavelengths [599 and 596 nm, Figs. 6(b) and 6(c), respectively], both $4d$ and $5s$ final states are accessible. Interferences are therefore observed for small distances [as in Fig. 6(d), final state $4d$] as

well as for large distances [as in Fig. 6(a), final state 5*s*]. For intermediate distances (between 12 and 14 cm), however, both interference patterns coexist, unlike in the simulations of Fig. 5 where the onsets of interferences are located at zero chirp (and the first maximum for small positive or negative chirp). Moreover, the interference patterns associated with each final state do not change when the laser wavelength is scanned. Only their relative weight depends on the wavelength. At first sight, these results seem to mean that the grating's position of "zero chirp" depends on the final state accessed instead of depending on the laser wavelength. However, a simulation based on the complete spectral phase of the excitation pulse (also shown in Fig. 6) fits perfectly the experimental results. The spectral phase introduced by the gratings is the following:

$$\phi_g(L,\omega) = 2\frac{\omega}{c}L\cos\,\theta_d(\omega), \tag{20}$$

where L is the distance between the two gratings (scanning parameter) and $\theta_d(\omega)$ the diffraction angle. The glass rods phase contribution is simply

$$\phi_r(\omega) = \frac{\omega}{c}[n_{\mathrm{SF58}}(\omega)L_{\mathrm{SF58}} + n_{\mathrm{SF10}}(\omega)L_{\mathrm{SF10}}]. \tag{21}$$

The excellent agreement between calculated and experimental results means that although the quadratic phase is sufficient to explain most of the observed phenomena, some details such as the position of the onset of interferences need higher-order terms to be explained. As detailed in Sec. V, including the effects of the cubic phase allows us to explain all the observed features.

V. EFFECT OF THE CUBIC PHASE

We have analyzed in the previous sections how the chirp associated to the quadratic phase allows clearly to separate the two different contributions (sequential and direct) to the two-photon absorption. The phase difference between these two quantum paths is proportional to the second-order phase derivative, so that varying the chirp allows one to scan the interference pattern. When a pure quadratic phase is taken into account, the interferences are present only for one sign of ϕ'' and start exactly at $\phi''=0$. This value corresponds to a Fourier-transform-limited (FT) pulse which maximizes the direct TPA. Also, changing the sign of ϕ'' changes the arrival order of the frequencies, so that the sequential path is allowed for one sign and forbidden for the other. However, the experimental results show that the onset of interferences corresponds to different spectral phase functions for different final states. These observations are in agreement with simulations including the whole spectral phase given by Eqs. (20) and (21). In order to understand qualitatively the observed features, we analyze in this section the role of the cubic phase [third order of dispersion (TOD)] and we show that the second and third orders are sufficient to explain all the observed features.

Taking into account the experimental parameters, the second- and third-order dispersions in our setup, for a given central frequency ω_0, are the following:

$$\phi''(L,\omega_0) = \phi_g''(L,\omega_0) + \phi_r'' = \frac{-L\alpha}{\omega_0^3} + \phi_r'', \tag{22}$$

$$\phi'''(L,\omega_0) = \phi_g'''(L,\omega_0) + \phi_r''' = \frac{3L\alpha}{\omega_0^4} + \phi_r''', \tag{23}$$

where $\alpha = 8\pi^2 c/d^2$ and $1/d$ is the number of grooves per millimeter. $\phi_g'''(L)$ and ϕ_r''' are positive quantities while $\phi_g''(L)$ and ϕ_r'' have opposite signs. So at the gratings' distance L_0 corresponding to $\phi''(L_0)=0$ the cubic phase has a significant value: the pulse is not FT limited. The analysis made above on the basis of all frequencies arriving either simultaneously in the pulse or, sequentially, is oversimplified to explain qualitatively the phenomena. Analytic expressions including the second and third orders of dispersion can be derived [70]. We show in the following how the use of Wigner representation can be helpful to understand the observed results.

A. Wigner representation

To have an intuitive understanding of the relations between time and frequency characteristics, several time-frequency distributions have been proposed [71]. The Wigner function has the simplest form among the usually used time-frequency distribution functions. Moreover, in the case of ultrashort pulses it can display features that bear a close relation to the instantaneous carrier frequency and group delay of the pulse, which makes it possible to analyze the laser chirp quantitatively [72]. For all these reasons the Wigner distribution is chosen for a better understanding of the role of higher-order terms of dispersion in the multiple interference pattern. The Wigner distribution for the electric field $E(\omega)$ in the frequency domain is defined as

$$W(t,\omega) = \frac{1}{\pi}\int E\left(\omega - \frac{\omega'}{2}\right)E^*\left(\omega + \frac{\omega'}{2}\right)e^{-i\omega' t}d\omega'. \tag{24}$$

The usefulness of this representation comes mainly from its marginal properties: the time marginal defined by the integration along the ω axis represents the intensity temporal profile and the frequency marginal defined by the integration along the t axis gives the spectral profile. As an example, the Wigner representation of a linearly chirped pulse is an ellipsis with a main axis corresponding approximately (in the limit of large chirps) to the instantaneous carrier frequency. For quadratic and cubic phases, the Wigner representation has a parabola shape: the instantaneous frequency is a nonlinear function of time or is not unique. More precisely, for small third-order spectral phases (compared to ϕ''), the parabola is a small deviation from the linear behavior [cf. Figs. 7(a), 7(b), 7(d), and 7(e)] whereas for pure cubic phase, the parabola is symmetric with respect to the time axis: Two instantaneous frequencies are simultaneously present in the pulse and vary symmetrically with respect to the central frequency [cf. Fig. 7(c)].

B. Application to our experiment

Figure 7 displays the Wigner function of the exciting pulse obtained for several values of the grating's distance L,

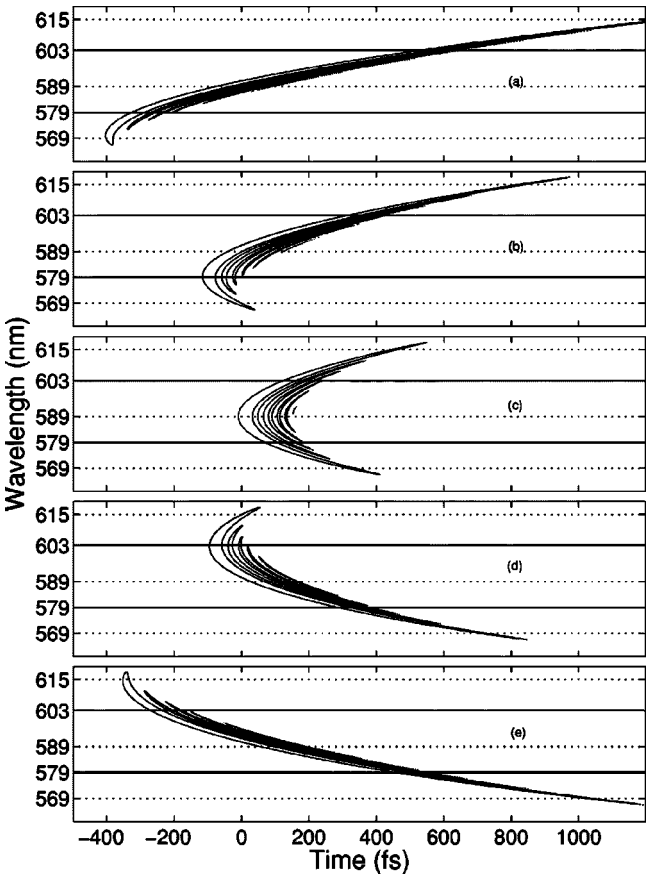

FIG. 7. Representation of the Wigner function of the excitation pulse, for one central wavelength (591 nm), such that both two-photon transitions are involved. Cases (a)–(e) represent the Wigner function for different values of the gratings' distance L_n such that $\phi''(\omega_n, L_n)=0$ where ω_n is a one-photon or two-photon resonance. (a) $L_a=15.48$ cm for which $\phi''(\omega_{3p\text{-}4d}, L_a)=0$, (b) $L_b=14.16$ cm for which $\phi''(\omega_{3s\text{-}4d}/2, L_b)=0$, (c) $L_c=13.0$ cm for which $\phi''(\omega_{3s\text{-}3p}, L_c)=0$, (d) $L_d=11.64$ cm for which $\phi''(\omega_{3s\text{-}5s}/2, L_d)=0$, and (e) $L_e=10.56$ cm for which $\phi''(\omega_{3p\text{-}5s}, L_e)=0$. One can note that 11.6 cm and 14.1 cm correspond to the onset of interferences in the experimental curves in Fig. 6. The horizontal solid lines correspond to the central wavelengths of the direct two-photon transitions whereas the horizontal dashed lines correspond to the wavelengths of the sequential contributions.

but with the same spectrum (centered at $\lambda=591$ nm, spectral width $\delta\lambda=30$ nm). These distances correspond to the different domains of interest which can be seen on Fig. 6. Namely, at intermediate distances ($11.7\ \text{cm} < L < 14.1$ cm), both final states can be accessed by sequential excitation. This case is illustrated in Fig. 7(c). At longer or shorter distances [Figs. 7(a) and 7(e)], only one final state can be reached by a sequential process. Finally, the plots on Figs. 7(b) and 7(d) correspond to the transition distances where the sequential path appears or disappears and where the direct path is maximized. These distances correspond to the main maxima observed in Fig. 6. More precisely, the characteristic gratings' distances L_k are chosen such that $\phi''(\omega_k, L_k)=0$ where ω_k is a one-photon or two-photon resonance (see Table I).

On each Wigner function plot, the wavelengths of these resonances are represented by horizontal lines. The vertices of the parabola correspond to these characteristic frequencies. At a given distance, in order to have a sequential contribution, the wavelengths of the one-photon transitions need to be correctly ordered within the pulse. The direct two-photon transitions are always maximized when the frequencies around the central two-photon frequencies arrive simultaneously. This is obviously the case for FT pulses. For non-FT pulses, having $\phi''(\omega_{eg}/2)=0$ provides a relative maximum for the direct two-photon process [cases shown in Figs. 7(b) and 7(d)].

In Figs. 7(a) and 7(e), all the frequencies involved (one and two-photon transitions) arrive sequentially in the pulse, corresponding effectively to a decreasing or increasing instantaneous frequency, respectively. The expected behavior is almost the same as for a quadratic phase only. As a matter of fact, the value of ϕ'' is such that it dominates the TOD.

In the intermediate cases [Figs. 7(b)–7(d)], due to the TOD, two "instantaneous frequencies" are simultaneously present. These frequencies start from the same initial value, vary in opposite directions, and finish at the lower end and higher end of the spectrum, respectively. This initial frequency decreases from Figs. 7(b)–7(d). It is respectively close to the $3s$-$4d$ two-photon transition [Fig. 7(b)], the $3s$-$3p$ transition [Fig. 7(c)], and the $3s$-$5s$ two-photon transition [Fig. 7(d)]. Thus, in Fig. 7(c), both sequential processes ($3s$-$3p$-$5s$ and $3s$-$3p$-$4d$) are fully allowed so that both interference patterns are present at the corresponding distance ($L_c=13.0$ cm; see Fig. 6). However, the direct two-photon processes are not maximized so that the interference contrast is not very high. When reducing the distance from $L_c=13.0$ cm, the initial frequency decreases and moves towards the frequency of the $3s$-$5s$ two-photon transition. When it reaches this value (at $L_d=11.64$ cm), the two frequencies $\omega_{3s\text{-}3p}$ and $\omega_{3p\text{-}5s}$ arrive simultaneously. This is the distance for which the sequential process (towards the $5s$ state) disappears. Slightly before this distance, one reaches the maximum of the $3s$-$3p$-$5s$ ladder. Similarly, when increasing the distance from $L_c=13.0$ cm, the initial frequency increases and moves towards the $3s$-$4d$ two-photon transition. At this value (for $L_b \simeq 14.16$ cm), the two frequencies $\omega_{3s\text{-}3p}$ and $\omega_{3p\text{-}4d}$ arrive simultaneously. Again, the sequential process towards the $4d$ state disappears, but slightly before this distance, the $3s$-$3p$-$4d$ ladder reaches its maximum.

The examples detailed here show the usefulness of the Wigner representation to understand the respective role of the quadratic and cubic spectral phase. An elegant explanation of the experimental observations based on the evolution of the instantaneous frequencies in the pulse could be given.

C. Optimization of the cubic phase

We have seen so far that the quadratic phase provides a sensitive way to adjust the interference phase between sequential and direct two-photon transitions. The first maximum appearing when scanning ϕ'' from $\phi''=0$ (with the correct sign) is also the absolute maximum. The effect of TOD can be intuitively seen as adding a "frequency dependence" to ϕ''. The condition for maximizing the direct two-photon path is given by $\phi''(\omega_{eg}/2)=0$. In case of second and third

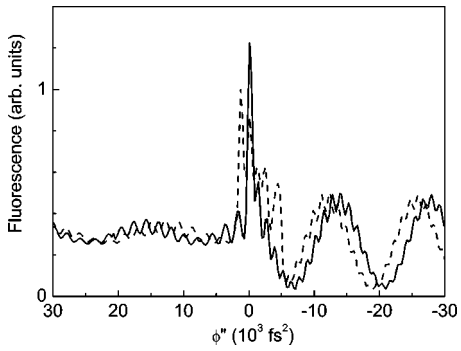

FIG. 8. Simulation of the $4p$-$3s$ fluorescence as a function of ϕ'' for the artificially reduced cubic phase (solid line) and, as a comparison, for the experimental cubic phase (dashed line). Here $\lambda = 596$ nm.

orders only phase dispersion, this condition corresponds also to the two sequential transitions arriving simultaneously.

As seen in the previous subsection, the transitions towards the two final states are not optimized simultaneously. Without any TOD, these maxima occur for slightly positive chirp (for the $4d$ final state) and for slightly negative chirp (for the $5s$ final state). With the TOD present in our experiment, these two maxima are strongly shifted in such a way that now the interference structures coexist for a given distance range instead of being separated. In this subsection, we decided to adjust artificially the amount of TOD in order to create a pulse shape which maximizes simultaneously the excitation towards both final states. In order to allow for a direct comparison with the present experiments, we have reduced the TOD of the system by a factor $\beta \simeq 0.2$, so that $\phi'''_{artif}(L) = \beta \phi'''(L)$ and we present in Fig. 8 a scan of the fluorescence yield obtained as a function of the gratings' distance L, together with the result obtained with the experimental parameters. With these new parameters, the two maxima (towards $4d$ and $5s$ final states) are now present for the same pulse parameters (gratings' distance). It should be recalled that since the paths associated to two different final states add incoherently, the maximum obtained is closed to the sum of the two contributions. In a real experiment, such pulse parameters could be achieved for instance by combination of dispersive rods, prism pairs, and gratings pairs or more easily with a pulse shaper [35,36,73].

VI. CONCLUSION

In this paper we have studied the role of the quadratic spectral phases of the excited pulse in a ladder climbing. This has been successfully demonstrated in sodium vapor. Due to the broad bandwidth of our laser, several two-photon transitions are allowed and eight quantum paths are involved leading to quantum interferences. A careful analysis based on the Wigner representation provides an elegant understanding of the complex interference pattern. The particular role of the cubic phase is emphasized. By carefully adjusting the relative values of the quadratic and cubic phases it is possible to maximize the effect of the two contributions.

As a conclusion, it is well known that in the case of a multiphoton transition without any resonant intermediate state, the expected results can be deduced from the power spectrum of $E^N(t)$ (for an N-photon transition) just as the result of a one-photon transition can be explained by the laser spectrum [38,43], provided that one is not interested by transients effects [41,44,74,75]. However, the presence of a nearly resonant intermediate state as in this work induces new subtle effects which require a careful analysis.

ACKNOWLEDGMENTS

We sincerely acknowledge Jean-Paul Pique for fruitful discussions on the artificial star project and the loan of the sodium cell and Sabine Stock for her participation at an earlier stage of the project.

[1] D. J. Tannor and S. A. Rice, J. Chem. Phys. **83**, 5013 (1985).
[2] P. Brumer and M. Shapiro, Chem. Phys. Lett. **126**, 541 (1986).
[3] M. Shapiro and P. Brumer, Int. Rev. Phys. Chem. **13**, 187 (1994).
[4] R. J. Gordon and S. A. Rice, Annu. Rev. Phys. Chem. **48**, 601 (1997).
[5] R. N. Zare, Science **279**, 1875 (1998).
[6] *Coherent Control in Atoms, Molecules and Semiconductors*, edited by W. Pötz and W. A. Schroeder (Kluwer Academic, Dordrecht, 1999).
[7] M. Shapiro and P. Brumer, Rep. Prog. Phys. **66**, 859 (2003).
[8] C. Chen, Y.-Y. Yin, and D. S. Elliott, Phys. Rev. Lett. **64**, 507 (1990).
[9] S. M. Park, S. P. Lu, and R. J. Gordon, J. Chem. Phys. **94**, 8622 (1991).
[10] L. Zhu, V. D. Kleiman, X. Li, S. P. Lu, K. Trentelman, and R. J. Gordon, Science **270**, 77 (1995).
[11] E. Dupont, P. B. Corkum, H. C. Liu, M. Buchanan, and Z. R. Wasilewski, Phys. Rev. Lett. **74**, 3596 (1995).
[12] R. Atanasov, A. Hache, J. L. P. Hughes, H. M. van Driel, and J. E. Sipe, Phys. Rev. Lett. **76**, 1703 (1996).
[13] U. Gaubatz, P. Rudecki, S. Schiemann, and K. Bergmann, J. Chem. Phys. **92**, 5363 (1990).
[14] N. V. Vitanov, T. Halfmann, B. W. Shore, and K. Bergmann, Annu. Rev. Phys. Chem. **52**, 763 (2001).
[15] A. H. Zewail, *Femtochemistry: Ultrafast Dynamics of the Chemical Bond* (World Scientific, Singapore, 1994).
[16] *Femtosecond Chemistry*, edited by J. Manz and L. Wöste (VCH, Weinheim, 1995).
[17] D. J. Tannor and S. A. Rice, J. Chem. Phys. **85**, 5805 (1986).
[18] E. D. Potter, J. L. Herek, S. Pedersen, Q. Liu, and A. H. Zewail, Nature (London) **355**, 66 (1992).
[19] J. T. Fourkas, W. L. Wilson, G. Wäckerle, A. E. Frost, and M. D. Fayer, J. Opt. Soc. Am. B **6**, 1905 (1989).
[20] N. F. Scherer, A. J. Ruggiero, M. Du, and G. R. Fleming, J. Chem. Phys. **93**, 856 (1990).

[21] L. D. Noordam, D. I. Duncan, and T. F. Gallagher, Phys. Rev. A **45**, 4734 (1992).
[22] J. Y. Bigot, M.-A. Mycek, S. Weiss, R. G. Ulbrich, and D. S. Chemla, Phys. Rev. Lett. **70**, 3307 (1993).
[23] R. R. Jones, C. S. Raman, D. W. Schumacher, and P. H. Bucksbaum, Phys. Rev. Lett. **71**, 2575 (1993).
[24] V. Blanchet, M. A. Bouchene, O. Cabrol, and B. Girard, Chem. Phys. Lett. **233**, 491 (1995).
[25] V. Blanchet, C. Nicole, M. A. Bouchene, and B. Girard, Phys. Rev. Lett. **78**, 2716 (1997).
[26] M. Bellini, A. Bartoli, and T. W. Hänsch, Opt. Lett. **22**, 540 (1997).
[27] X. Marie, P. Le Jeune, T. Amand, M. Brousseau, J. Barrau, M. Paillard, and R. Planel, Phys. Rev. Lett. **79**, 3222 (1997).
[28] R. Netz, A. Nazarkin, and R. Sauerbrey, Phys. Rev. Lett. **90**, 063001 (2003).
[29] K. Ohmori, Y. Sato, E. E. Nikitin, and S. A. Rice, Phys. Rev. Lett. **91**, 243003 (2003).
[30] R. Kosloff, S. A. Rice, P. Gaspard, S. Tersigni, and D. J. Tannor, Chem. Phys. **139**, 201 (1989).
[31] R. S. Judson and H. Rabitz, Phys. Rev. Lett. **68**, 1500 (1992).
[32] A. Assion, T. Baumert, M. Bergt, T. Brixner, B. Kiefer, V. Seyfried, M. Strehle, and G. Gerber, Science **282**, 919 (1998).
[33] R. J. Levis, G. M. Menkir, and H. Rabitz, Science **292**, 709 (2001).
[34] C. Daniel, J. Full, L. Gonzalez, C. Lupulescu, J. Manz, A. Merli, S. Vajda, and L. Wöste, Science **299**, 536 (2003).
[35] P. Tournois, Opt. Commun. **140**, 245 (1997).
[36] A. M. Weiner, Rev. Sci. Instrum. **71**, 1929 (2000).
[37] D. Meshulach and Y. Silberberg, Nature (London) **396**, 239 (1998).
[38] D. Meshulach and Y. Silberberg, Phys. Rev. A **60**, 1287 (1999).
[39] T. Hornung, R. Meier, D. Zeidler, K.-L. Kompa, D. Proch, and M. Motzkus, Appl. Phys. B: Lasers Opt. **71**, 277284 (2000).
[40] N. Dudovich, B. Dayan, S. M. Gallagher Faeder, and Y. Silberberg, Phys. Rev. Lett. **86**, 47 (2001).
[41] J. Degert, W. Wohlleben, B. Chatel, M. Motzkus, and B. Girard, Phys. Rev. Lett. **89**, 203003 (2002).
[42] J. B. Ballard, H. U. Stauffer, E. Mirowski, and S. R. Leone, Phys. Rev. A **66**, 043402 (2002).
[43] V. V. Lozovoy, I. Pastirk, K. A. Walowicz, and M. Dantus, J. Chem. Phys. **118**, 3187 (2003).
[44] W. Wohlleben, J. Degert, A. Monmayrant, B. Chatel, M. Motzkus, and B. Girard, Appl. Phys. B: Lasers Opt. **79**, 435 (2004).
[45] S. Chelkowski, A. D. Bandrauk, and P. B. Corkum, Phys. Rev. Lett. **65**, 2355 (1990).
[46] S. Guérin, Phys. Rev. A **56**, 1458 (1997).
[47] D. J. Maas, D. I. Duncan, A. F. G. van der Meer, W. J. van der Zande, and L. D. Noordam, Chem. Phys. Lett. **270**, 45 (1997).
[48] D. J. Maas, M. J. J. Vrakking, and L. D. Noordam, Phys. Rev. A **60**, 1351 (1999).
[49] G. von Helden, I. Holleman, G. Meijer, and B. Sartakov, Opt. Express **4**, 2 (1999).
[50] B. Y. Chang, I. R. Sola, and J. Santamaria, J. Phys. Chem. A **105**, 8864 (2001).
[51] T. Witte, T. Hornung, L. Windhorn, D. Proch, R. de Vivie-Riedle, M. Motzkus, and K. L. Kompa, J. Chem. Phys. **118**, 2021 (2003).
[52] C. Ventalon, J. M. Fraser, M. H. Vos, A. Alexandrou, J.-L. Martin, and M. Joffre, Proc. Natl. Acad. Sci. U.S.A. **101**, 13216 (2004).
[53] D. M. Villeneuve, S. A. Aseyev, P. Dietrich, M. Spanner, M. Y. Ivanov, and P. B. Corkum, Phys. Rev. Lett. **85**, 542 (2000).
[54] N. V. Vitanov and B. Girard, Phys. Rev. A **69**, 033409 (2004).
[55] B. Broers, H. B. van Linden van den Heuvell, and L. D. Noordam, Phys. Rev. Lett. **69**, 2062 (1992).
[56] P. Balling, D. J. Maas, and L. D. Noordam, Phys. Rev. A **50**, 4276 (1994).
[57] D. J. Maas, C. W. Rella, P. Antoine, E. S. Toma, and L. D. Noordam, Phys. Rev. A **59**, 1374 (1999).
[58] A. Assion, T. Baumert, J. Helbing, V. Seyfried, and G. Gerber, Chem. Phys. Lett. **259**, 488 (1996).
[59] B. Chatel, J. Degert, S. Stock, and B. Girard, Phys. Rev. A **68**, 041402R (2003).
[60] M. Hentschel *et al.*, Nature (London) **414**, 509 (2001).
[61] G. G. Paulus, F. Lindner, H. Walther, A. Baltuska, E. Goulielmakis, M. Lezius, and F. Krausz, Phys. Rev. Lett. **91**, 253004 (2003).
[62] F. Lindner, G. G. Paulus, H. Walther, A. Baltuska, E. Goulielmakis, M. Lezius, and F. Krausz, Phys. Rev. Lett. **92**, 113001 (2004).
[63] C. E. Moore, *Atomic Energy Levels* (U. S. GPO, Washington, DC, 1971).
[64] I. I. Sobelman, *Atomic Spectra and Radiative Transitions*, 2nd ed. (Springer, Berlin, 1992).
[65] M. A. Bouchene, V. Blanchet, C. Nicole, N. Melikechi, B. Girard, H. Ruppe, S. Rutz, E. Schreiber, and L. Wöste, Eur. Phys. J. D **2**, 131 (1998).
[66] C. Nicole, M. A. Bouchene, C. Meier, S. Magnier, E. Schreiber, and B. Girard, J. Chem. Phys. **111**, 7857 (1999).
[67] S. Zamith, M. A. Bouchene, E. Sokell, C. Nicole, V. Blanchet, and B. Girard, Eur. Phys. J. D **12**, 255 (2000).
[68] E. Sokell, S. Zamith, M. A. Bouchene, and B. Girard, J. Phys. B **33**, 2005 (2000).
[69] E. Riedle, M. Beutter, S. Lochbrunner, J. Piel, S. Schenkl, S. Spörlein, and W. Zinth, Appl. Phys. B: Lasers Opt. **71**, 457 (2000).
[70] C. Leichtle, I. S. Averbukh, and W. P. Schleich, Phys. Rev. A **54**, 5299 (1996).
[71] J. Paye and A. Migus, J. Opt. Soc. Am. B **12**, 1480 (1995).
[72] K.-H. Hong, J.-H. Kim, Y. H. Kang, and C. H. Nam, Appl. Phys. B: Lasers Opt. **74**, 231 (2002).
[73] A. Monmayrant and B. Chatel, Rev. Sci. Instrum. **75**, 2668 (2004).
[74] S. Zamith, J. Degert, S. Stock, B. de Beauvoir, V. Blanchet, M. A. Bouchene, and B. Girard, Phys. Rev. Lett. **87**, 033001 (2001).
[75] N. Dudovich, D. Oron, and Y. Silberberg, Phys. Rev. Lett. **88**, 123004 (2002).